Earth and Planetary Science Letters 428 (2015) 204–216

Contents lists available at ScienceDirect

Earth and Planetary Science Letters

www.elsevier.com/locate/epsl

# Pacific $^{187}Os/^{188}Os$ isotope chemistry and U–Pb geochronology: Synchroneity of global Os isotope change across OAE 2

A.D.C. Du Vivier [a,*], D. Selby [a], D.J. Condon [b], R. Takashima [c], H. Nishi [c]

[a] Department of Earth Sciences, Durham University, Durham, DH1 3LE, UK
[b] NERC Isotope Geosciences Laboratory, British Geological Survey, Keyworth, NG12 5GG, UK
[c] The Centre for Academic Resources and Archives Tohoku University Museum, Tohoku University, Aramaki Aza Aoba 603, Aoba-ku, Sendai, 980-8578, Japan

ARTICLE INFO

*Article history:*
Received 9 August 2014
Received in revised form 20 June 2015
Accepted 9 July 2015
Available online 3 August 2015
Editor: G.M. Henderson

*Keywords:*
Oceanic Anoxic Event 2
late cretaceous
U–Pb geochronology
palaeocirculation
global framework

ABSTRACT

Studies of OAE 2 sections beyond the Atlantic Ocean, Western Interior Seaway (WIS) and European pelagic shelf are limited. Here, we present initial osmium isotope stratigraphy ($^{187}Os/^{188}Os$–$Os_i$) from two proto-Pacific sites that span the Cenomanian–Turonian boundary interval (CTBI): the Yezo Group (YG) section, Hokkaido, Japan, and the Great Valley Sequence (GVS), California, USA; to evaluate the $^{187}Os/^{188}Os$ seawater chemistry of the proto-Pacific. Additionally we combine new $^{206}Pb/^{238}U$ zircon CA-ID-TIMS geochronology from five volcanic tuff horizons of the Yezo Group section to test and facilitate inter-basinal integration with the WIS using radio-isotopically constrained age–depth models for both sections, and quantitatively constrain the absolute timing and duration of events across the CTBI.

The YG shows an almost identical $Os_i$ profile to that of the WIS, and very similar to that of other sites of the proto-Atlantic and European pelagic oceans (Turgeon and Creaser, 2008; Du Vivier et al., 2014). The characteristics of the $Os_i$ profile are radiogenic and heterogeneous (~0.55–0.85) prior to the OAE 2, and synchronous with the inferred OAE 2 onset the $Os_i$ abruptly become unradiogenic and remain relatively homogeneous (~0.20–0.30) before showing a gradual return to more radiogenic $Os_i$ (~ 0.70) throughout the middle to late OAE 2. A $^{206}Pb/^{238}U$ zircon age of an interbedded tuff (HK017) in the adjacent horizon to the first unradiogenic $Os_i$ value constrains the age of the $Os_i$ inflection at $94.44 \pm 0.14$ Ma. This age, including uncertainty, agrees with the interpolated age of the same point in the $Os_i$ profile ($94.28 \pm 0.25$ Ma) in the only other dated OAE 2 section, the WIS; indicating a coeval shift in seawater chemistry associated with volcanism at the OAE 2 onset at the levels of temporal resolution (ca. 0.1 Myr). Further, prior to the onset of OAE 2 an enhanced radiogenic inflection in the $Os_i$ profile of the YG is correlative, within uncertainty, with a similar trend in the WIS based on the U–Pb age–depth model. The interpolated ages, $94.78 \pm 0.12$ Ma and $94.66 \pm 0.25$ Ma for this $Os_i$ inflection in the YG and WIS, respectively, indicate that palaeocirculation was sufficient to simultaneously influence transbasinal seawater chemistry. In contrast, the pre-OAE 2 $Os_i$ profile for the GVS is disparate to that of the YG and those of the proto-Atlantic and European pelagic shelf locations. We interpret the pre OAE 2 heterogeneous $Os_i$ values (0.30–0.95) to record a palaeobasin that was regionally influenced interchangeably by both unradiogenic (hydrothermal flux) and radiogenic (continental flux) Os.

We conclude that the $Os_i$ profiles from the proto-Pacific sections record both trends that are consistent globally (OAE 2 onset, syn and post OAE 2), but also show regional differences (pre OAE 2) between OAE 2 sections worldwide. As such the $Os_i$ profiles coupled with U–Pb geochronology facilitate the correlation of OAE 2 stratigraphy, and demonstrate both regional and global ocean dynamics.



## 1. Introduction

Oceanic anoxic events (OAEs) are a consequence of an imbalance to a sensitive global ocean–atmosphere system, which result in episodes of oxygen depletion in the oceans (Jenkyns, 2010). They are characterised by the accumulation of organic-rich material, commonly associated with biodiversity decline and/or extinctions in the biostratigraphic record, and typically identified by a 2–4‰ positive shift in the $\delta^{13}C$ record (Jenkyns, 2010). Such characteristics are representative of OAE 2, which occurred during the late Cretaceous across the Cenomanian–Turonian boundary (CTB, 93.90 Ma) and is hypothesised to have influenced basinal

* Corresponding author.
*E-mail addresses:* duviv510@hotmail.com (A.D.C. Du Vivier), david.selby@durham.ac.uk (D. Selby).

http://dx.doi.org/10.1016/j.epsl.2015.07.020

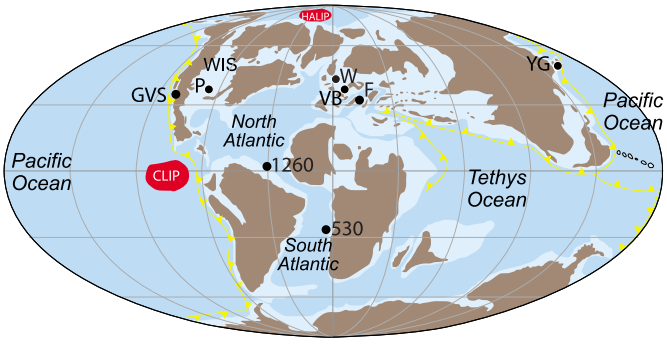


**Fig. 1.** Palaeogeographic map illustrating sample locations discussed in this study and previous studies (Turgeon and Creaser, 2008; Du Vivier et al., 2014). Locations: YG – Yezo Group, Hokkaido (Japan); GVS – Great Valley Sequence, California (USA); P – Portland #1 Core, Colorado (USA) (WIS – Western Interior Seaway); W – Wunstorf (Germany); VB – Vocontian Basin (SE France); F – Furlo (Italy); 1260 – Site 1260 B, Demerara Rise, (North Atlantic); 530 – Site 530 A, Angola Basin (South Atlantic). The High Arctic and Caribbean Large Igneous Provinces are marked on the map as HALIP and CLIP (Zheng et al., 2013).

environments at a global scale (Jenkyns, 1980; Schlanger et al., 1987). This hypothesis is based on studies that have predominately focused on a globally narrow region, e.g., the proto-Atlantic, European pelagic shelf and Western Interior Sea (WIS). To date, analysis of OAE 2 sections recording deposition from basins of the Cretaceous World's largest water mass, the proto-Pacific, are limited and have predominately focused on $\delta^{13}C$ records in comparison to the multi-element/isotope studies of the proto-Atlantic, European pelagic shelf and WIS (Kaiho et al., 1993; Hasegawa and Saito, 1993; Hasegawa, 1995, 1999; Tamaki and Itoh, 2008; Takashima et al., 2004, 2011; Quidelleur et al., 2011). The main reasons for the limited studies are the poor preservation and the uncertainty of stratigraphic location of the OAE 2 record. Two sites that represent a complete record of OAE 2 from deposition in the proto-Pacific are the Yezo Group (YG) section, Hokkaido, Japan and the Great Valley Sequence (GVS), California, USA (Fig. 1). Herein we report and discuss the implications of the Os isotope data (YG and GVS) and U–Pb zircon geochronology (YG only) for these sites.

The identification and correlation of OAE 2 is fundamentally based upon the carbon isotope record combined with biostratigraphy and subordinate radio-isotopic dating. Here we apply the traditional $\delta^{13}C$ datum levels for correlation to both the YG and the GVS sections, where peaks and troughs in the $\delta^{13}C$ record are associated with bioevents and changes in lithology. The sections are commonly correlated according to this method using certain inflection points ('A', 'B' and 'C') of the $\delta^{13}C$ curve that are similar to those first defined by Pratt et al. (1985) in the WIS for the GSSP and refined later by Tsikos et al. (2004); where 'A' represents the last value of relatively depleted $\delta^{13}C$ before the first major shift to positive values; the base of the excursion marks the onset of OAE 2 (Pratt et al., 1985); 'B' marks the trough of depleted values following the positive excursion in the $\delta^{13}C$ record (Pratt et al., 1985); and 'C' denotes the end of the 'plateau', the last relatively enriched value prior to the $\delta^{13}C$ trending back to pre-OAE 2 values (Tsikos et al., 2004). Since the discovery of OAEs, a number of isotopic/elemental proxies that are sensitive to the chemical perturbations (e.g. Sr, Os, Ca, Nd, P, Pb, Li, U, S; Arthur et al., 1987; McArthur et al., 2004; Forster et al., 2007; MacLeod et al., 2008; Turgeon and Creaser, 2008; Voigt et al., 2008; Montoya-Pino et al., 2010; Blättler et al., 2011; Kuroda et al., 2011; Mort et al., 2011; Pogge von Strandmann et al., 2013; Owens et al., 2013; Du Vivier et al., 2014, 2015) have aided the understanding of the driving mechanisms of oceanic anoxia, and deciphering responses of seawater chemistry in multiple basin environments.

The osmium (Os) isotope composition of seawater (expressed as $^{187}Os/^{188}Os$) reflects the mixing of radiogenic Os weathered from ancient continental crust ($^{187}Os/^{188}Os = \sim 1.4$; Peucker-Ehrenbrink and Jahn, 2001), and unradiogenic Os from mantle (hydrothermal) and extraterrestrial sources ($^{187}Os/^{188}Os = 0.12$; Peucker-Ehrenbrink and Ravizza, 2000). The $^{187}Os/^{188}Os$ measurements of organic-carbon enriched marine sedimentary sections provide a means of determining the $^{187}Os/^{188}Os$ of seawater at the time of deposition through the calculated initial $^{187}Os/^{188}Os$ value ($Os_i$) from the measured Re–Os isotope compositions of a sedimentary unit (Cohen et al., 1999). The latter, coupled with the short residence time of Os in seawater ($\leq$10 kyr; Oxburgh, 2001), has shown the potential of providing global correlations via $^{187}Os/^{188}Os$ stratigraphy throughout many OAE 2 proto-Atlantic and European sections (Turgeon and Creaser, 2008; Du Vivier et al., 2014). However, hitherto $Os_i$ data for the proto-Pacific OAE 2 sections is lacking. Here we present $Os_i$ stratigraphy from the YG section, Japan and the GVS, USA (Fig. 1). Further, to objectively compare and evaluate if the $Os_i$ trends from the proto-Pacific are similar and/or temporally identical, and therefore assess the truly global extent of OAE 2 on ocean chemistry with that of the WIS, proto-Atlantic and European pelagic shelf, we present chemical abrasion isotope dilution thermal ionisation mass spectrometry (CA-ID-TIMS) $^{206}Pb/^{238}U$ zircon geochronology of interbedded tuff horizons of the YG section. The latter is essential given that, with the exception of the WIS where absolute geochronology of volcanic tuff horizons from multiple locations, together with bio- and cyclic-stratigraphy, have been integrated to nominally constrain the absolute chronology of the Cenomanian–Turonian boundary interval (CTBI) of the Portland #1 core (Meyers et al., 2012a), OAE 2 sites are unsupported by absolute dating.

In addition to using the most current analytical protocols (e.g., chemical abrasion, Mattinson, 2005) we also use the EARTHTIME U–Pb tracer solutions (Condon et al., 2015; McLean et al., 2015) to provide absolute temporal constraints for the YG to present a potential OAE 2 reference section for the proto-Pacific Ocean. We also construct a $^{206}Pb/^{238}U$ zircon based age–depth model to help constrain integrated sediment accumulation rates for the YG section OAE 2 interval, which in turn permits a quantitative estimate for the duration of events across the CTBI. The YG age–depth model permits quantitative comparison with the WIS records to assess synchroneity of the OAE 2 onset as well as events highlighted in $Os_i$ chemostratigraphy during the pre-OAE 2 interval, and thus provides evidence of water mass exchange and palaeocirculation during the CTBI (see Discussion).

## 2. Geological setting and stratigraphy

### 2.1. Yezo Group (YG), Hokkaido, Japan

The YG was deposited along an active continental margin in an arc-trench system at ~45°N along the Eurasian margin during the late Mesozoic (Tamaki and Itoh, 2008; Fig. 1). The 300 km N–S trending trench acted as a depositional basin for the YG and the sediments accumulated at shallow marine-bathyal depths in a continental slope environment (Kaiho et al., 1993; Takashima et al., 2004). Post deposition the YG was compacted and then tilted by the late Tertiary rotation of the Japan Sea back-arc basin (Tamaki and Itoh, 2008). The YG records a conformable sequence determined through bioevents and sedimentary structures (Kaiho et al., 1993). The OAE 2 section of the YG is part of the Saku Formation and outcrops on the Hakkin River, at Oyubari, on Hokkaido at ~142°9′27″E, 43°2′44″N. The 300 m exposed OAE 2 section of the Saku Formation is represented in part by the Hakkin muddy-sandstone member and comprises dark-grey organic-rich terrigenous sandy siltstone, bedded conglomeritic turbidites and

finely laminated pyrite-rich green–grey mudstone possessing 0.5 to 1 wt.% TOC (Fig. 2; Takashima et al., 2004). In addition, multiple thin and thick (0.02–2 m) felsic volcanic tuffs are interbedded throughout the sequence (Fig. 2; Takashima et al., 2004, 2011), which are locally altered to bentonite (Takashima et al., 2004). There are no documented hiatuses in the YG section (Takashima et al., 2011).

The Oyubari YG section contains sufficient stratigraphic indicators for high-resolution global correlation of OAE 2, making it a key regional reference section for the NW Pacific (Hasegawa, 1995; Fig. 2; see Supplementary Material). Worldwide correlation and the identification of the CTB is dependent upon the identification of *W. archaeocretacae*; however the absence of *W. archaeocretacae* and the rare occurrence of *H. Helvetica*, means that the FO of *M. schneegansi* is used to identify the base of the Turonian in the YG (Fig. 2; Takashima et al., 2010).

The $\delta^{13}C_{wood}$ profile represents a 5-point moving average (Fig. 2; Takashima et al., 2011). The $\delta^{13}C_{wood}$ record is correlated with the Pont d'Issole section of the Vocontian Basin through the characteristic datum levels: 'A', 'B', and 'C' (Takashima et al., 2011), however the nature of the $\delta^{13}C_{wood}$ record results in significant stratigraphic uncertainty in the position of these datum levels in the YG record. The stratigraphic position of the OAE 2 onset is given at −39 m (Fig. 2; "original identification onset A"; Takashima et al., 2011). The $\delta^{13}C_{wood}$ reaches a maximum of −19.3‰ (Fig. 2; Takashima et al., 2011) before the decline in $\delta^{13}C_{wood}$ values to 'B'. The $\delta^{13}C_{wood}$ values across the 'plateau' up to 'C' are less enriched in this section compared to other OAE 2 sites (e.g., GVS; Takashima et al., 2011). As such, the profile records a continuous gradual trend to pre-OAE 2 $\delta^{13}C_{wood}$ values (∼ −24.5‰), which could be a reflection of the homogeneous nature of the deposits throughout the duration of OAE 2. Here we discuss and re-evaluate the stratigraphic position of the OAE 2 onset and the CTB in the YG section using $Os_i$ stratigraphy and U–Pb geochronology (Fig. 2; see Discussion).

Two tuff horizons from the YG CTBI have provided imprecise and stratigraphically inconsistent $^{206}Pb/^{238}U$ zircon dates (Fig. 2 in green; Quidelleur et al., 2011). Tuff HKt002 located above the last occurrence of *R. cushmani* (Upper Cenomanian) possesses a LA-ICP-MS U–Pb zircon date of 92.9 ± 1.3 Ma ($n = 16$), with a stratigraphically younger tuff (HKt003) generating an older U–Pb multi-grain ID-TIMS age of 94.3 ± 0.3 Ma ($n = 7$; MSWD = 1.5). The level of uncertainty for these U–Pb dates for the YG are problematic based on the $^{40}Ar/^{39}Ar$ calibrated age model of the OAE 2 from the WIS, which constrains the CTB to 93.90 ± 0.15 Ma (Meyers et al., 2012a). Given the OAE 2 temporal constraints, the dated horizon HKt002 and HKt003 of the YG should be >93.9 Ma (Fig. 2; see Discussion). The large uncertainty (1.4%) of the interpreted HKt002 date is intrinsic to the analytical method making it of little use for resolving the issues related to the timing of OAE 2, which occurred over an interval of <1 Myr. As such we do not include the current U–Pb zircon dates for integration at the sub 0.5 Myr level for our age–depth model of the YG (see Discussion).

### 2.2. Great Valley Sequence (GVS), California, Western USA

Similar to the YG, the GVS was deposited along an active continental margin: ∼30–40°N on the North American continental fore arc margin in upper bathyal depths (Fernando et al., 2011), and is now exposed along the western border of the Sacramento Valley (Fig. 1). The Budden Canyon Formation records sedimentary deposition from the Berriasian to the Turonian and consists of 7 mappable units throughout road cuttings 122°33′02″W, 40°26′30″N in California (Murphy et al., 1969; Fernando et al., 2011); the youngest and uppermost unit is the Gas Point Member, ∼730 m thick, which records the CTB and the OAE 2. The OAE 2 stratigraphy is recognised by elevated TOC (0.5–1.0 wt.%; Takashima et al., 2011). The GVS OAE 2 interval is dominated by dark-grey organic-rich terrigenous mudstone with some thinly bedded turbidites and minor conglomerate sandstone horizons becoming more frequent up sequence (Murphy et al., 1969; Takashima et al., 2011). There are no documented hiatuses in the GVS section (Takashima et al., 2011).

The deposition of the GVS in a fore arc basin (Fernando et al., 2011) is dissimilar to the other OAE 2 sites; i.e., the WIS is an epeiric sea. As a result there is an absence and/or variability in abundance, distribution and duration of biozone horizons. The LO of *R. cushmani* is identified at 80 m in the section, ∼30 m in to the OAE 2 interval. The FO *Q. gartneri* marks the basal Turonian at ∼315 m in the section which occurs ∼265 m above the OAE 2 onset (Fig. 2; Takashima et al., 2011; see Supplementary Material for detail).

In the GVS section the $\delta^{13}C_{wood}$ curve is presented like YG as a 5-point moving average (Fig. 2), however the record is less variable than the YG $\delta^{13}C_{wood}$ record and depicts a more typical convex trend despite the subtle 1.2‰ VPDB positive excursion (Fig. 2; Takashima et al., 2011). As a result of the lower variability of the $\delta^{13}C_{wood}$ curve, correlation with the Pont d'Issole section through datum levels 'A', 'B' and 'C' is more robust than for the YG section. The excursion marks the onset of OAE 2 at datum level 'A' (49 m; Fig. 2) from −24.5‰ to −23.3‰. The trough at 'B' is followed by a gradual enrichment to −20.8‰, where the 'plateau' of enriched $\delta^{13}C_{wood}$ values continues up to 'C'. In the GVS the OAE 2 is recorded throughout an expanded section, ∼201 m; after datum level 'C' the $\delta^{13}C_{wood}$ values return to pre-OAE 2 values of ∼ −23.5‰ (Fig. 2; Takashima et al., 2011).

## 3. Analytical protocol

### 3.1. Re–Os geochemistry

The hydrogenous $Os_i$ composition of the TOC-rich sample set was achieved through the established methodology of Selby and Creaser (2003; see Supplementary Material) at Durham University. This protocol has been shown to significantly limit the detrital component of Re and Os (e.g., Selby and Creaser, 2003; Kendall et al., 2004; Rooney et al., 2011; Kendall et al., 2013).

### 3.2. U–Pb zircon geochronology

All $^{206}Pb/^{238}U$ zircon geochronology preparation, analysis and processing was conducted at NIGL (NERC Isotope Geosciences Laboratory). We have applied established analytical methodology (e.g., Sageman et al., 2014) for $^{206}Pb/^{238}U$ zircon ID-TIMS (see Supplementary Material for detail). All $^{206}Pb/^{238}U$ dates (ID-TIMS) were calculated using the ET2535 mixed U–Pb tracer (Condon et al., 2015; McLean et al., 2015) and the $^{238}U$ and $^{235}U$ decay constants of Jaffey et al. (1971). The $^{238}U/^{235}U_{zircon}$ value of 137.818 ± 0.045 (Hiess et al., 2012) was used in the data reduction calculations for ID-TIMS dates (see Tables 1a and 1b). Data reduction was carried out using U–Pb REDUX (McLean et al., 2011).

## 4. Results and interpretation

### 4.1. Re–Os abundance

The Re abundance for the YG ranges from ∼0.20 to ∼1.60 ppb and from ∼0.25 to ∼3.75 ppb for the GVS (Supplementary Material Tables 1a, 1b). These values are similar to other OAE 2 sections (Turgeon and Creaser, 2008; Du Vivier et al., 2014). Across the onset of OAE 2 there is a noticeable shift to an increase in the abundance of common Os, i.e., non-radiogenic generated Os, which is denoted by $^{192}Os$ (Turgeon and Creaser, 2008;

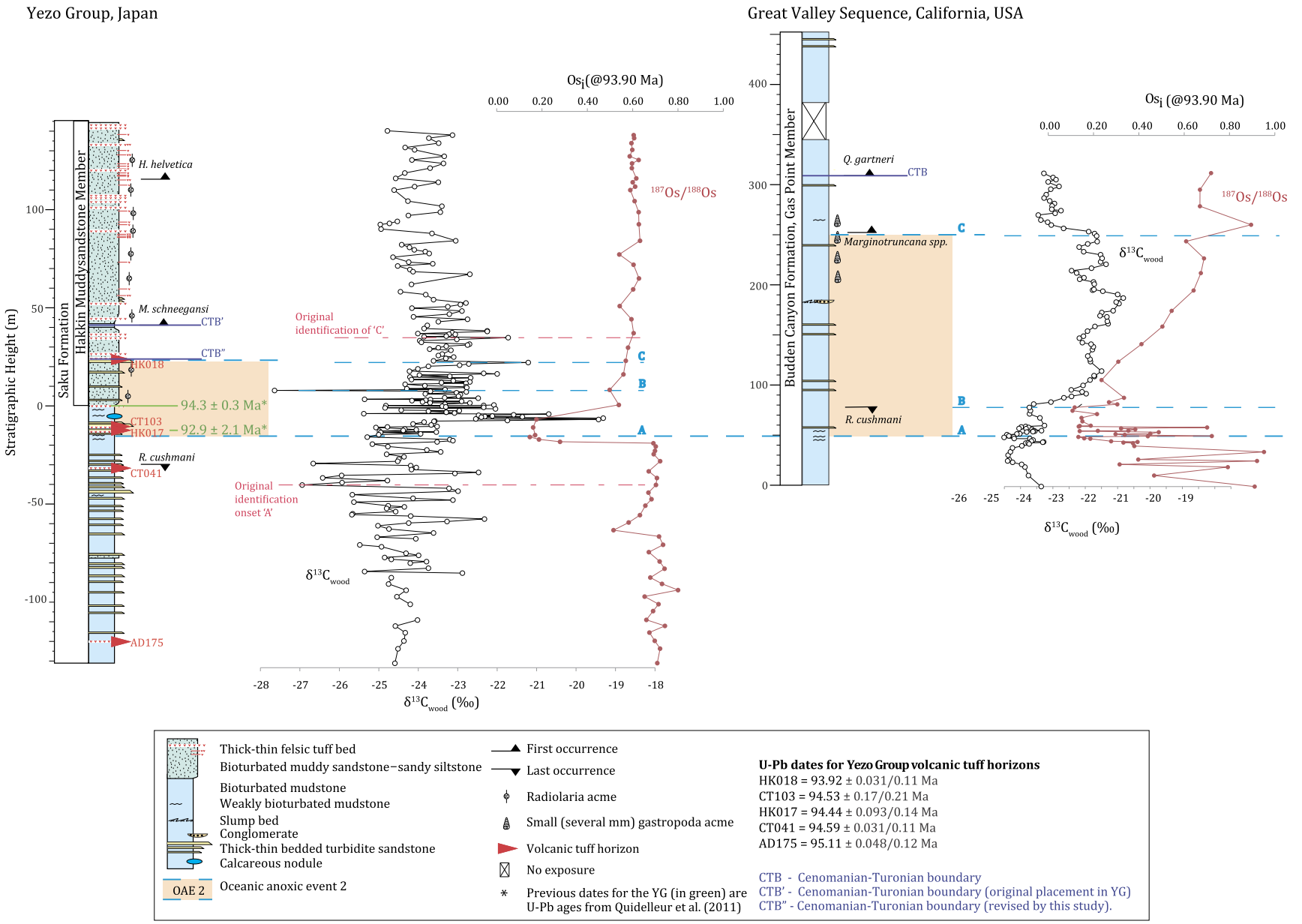


**Fig. 2.** Stratigraphic columns for Yezo Group, Japan and Great Valley Sequence, California, USA – Cenomanian–Turonian boundary identified based on biozones. CTB' denotes the CTB according to Takashima et al. (2011). CTB" denotes the revision of the CTB according to U–Pb ages (see Discussion). Volcanic tuff horizons for U–Pb zircon dating are marked on the Yezo Group. The OAE 2 interval is shaded in orange. Initial $^{187}Os/^{188}Os$ profiles are in red. The correlated datum levels 'A', 'B', 'C' inferred from a combination of litho-, bio-, and chemostratigraphy and the extrapolated age of the onset of OAE 2 (Du Vivier et al., 2014), are shown in blue (see text for discussion). The stratigraphic height of the U–Pb dated tuff horizons from the Yezo Group, Japan are marked by red triangles. The existing U–Pb ages, with total uncertainties, for the Yezo Group are in green ($2\sigma$; Quidelleur et al., 2011). The stratigraphic thickness of the OAE 2 interval (shaded) reflects a variation of the chemostratigraphic approach defining widely recognised elements of the C isotope excursion (A, B, and C datum levels).

**Table 1a**
U–Pb zircon CA-ID-TIMS data for tuff horizons throughout the Cenomanian–Turonian boundary interval, Yezo Group, Japan.

| Fraction zircon | Composition | | | | Isotopic ratios | | | | | | | | | Dates (Ma) | | | | | |
|---|---|---|---|---|---|---|---|---|---|---|---|---|---|---|---|---|---|---|---|
| | Pb* (pg)[a] | Pb*/Pbc[b] | Pbc (pg)[c] | Th/U[d] | $^{206}Pb/^{204}Pb$[e] | $^{206}Pb/^{238}U$[f,g] | ±2σ (%) | $^{207}Pb/^{235}U$[f] | ±2σ (%) | $^{207}Pb/^{206}Pb$[f] | ±2σ (%) | Corr. coef. | % disc[h] | $^{206}Pb/^{238}U$[g] | ±2σ abs | $^{207}Pb/^{235}U$[i] | ±2σ abs | $^{207}Pb/^{206}Pb$[g] | ±2σ abs |
| HK018 | | | | | | | | | | | | | | | | | | | |
| _1_z1 | 21.66 | 24.04 | 0.90 | 0.57 | 1450 | 0.014690 | 0.04 | 0.096877 | 0.21 | 0.047895 | 0.20 | 0.418 | −0.948 | 94.008 | 0.04 | 93.889 | 0.19 | 93.0 | 4.8 |
| _2_z1B | 15.17 | 12.01 | 1.26 | 0.57 | 733 | 0.014672 | 0.06 | 0.096595 | 0.45 | 0.047814 | 0.42 | 0.493 | −5.378 | 93.895 | 0.05 | 93.628 | 0.40 | 89.0 | 10.0 |
| _2_z3 | 12.66 | 12.09 | 1.05 | 0.64 | 725 | 0.014700 | 0.19 | 0.096906 | 0.71 | 0.047874 | 0.61 | 0.624 | −2.173 | 94.075 | 0.18 | 93.917 | 0.64 | 92.0 | 14.5 |
| z1 | 28.66 | 20.14 | 1.42 | 0.66 | 1188 | 0.014704 | 0.08 | 0.096933 | 0.32 | 0.047876 | 0.28 | 0.614 | −2.096 | 94.096 | 0.07 | 93.941 | 0.29 | 92.1 | 6.6 |
| z2 | 38.22 | 33.02 | 1.16 | 0.65 | 1942 | 0.014700 | 0.06 | 0.097137 | 0.20 | 0.047990 | 0.16 | 0.665 | 3.822 | 94.071 | 0.06 | 94.130 | 0.18 | 97.7 | 3.9 |
| z5 | 40.68 | 18.01 | 2.26 | 0.71 | 1053 | 0.014693 | 0.15 | 0.097096 | 0.38 | 0.047990 | 0.31 | 0.615 | 3.846 | 94.030 | 0.14 | 94.092 | 0.34 | 97.7 | 7.3 |
| z6A | 10.16 | 33.30 | 0.30 | 0.53 | 2019 | 0.014688 | 0.04 | 0.096752 | 0.22 | 0.047842 | 0.21 | 0.284 | −3.882 | 93.994 | 0.03 | 93.774 | 0.19 | 90.4 | 4.9 |
| z6B | 20.37 | 37.78 | 0.54 | 0.56 | 2270 | 0.014680 | 0.04 | 0.096592 | 0.18 | 0.047787 | 0.16 | 0.479 | −7.050 | 93.945 | 0.04 | 93.626 | 0.16 | 87.7 | 3.9 |
| z7B | 24.03 | 51.56 | 0.47 | 0.63 | 3037 | 0.014710 | 0.04 | 0.097140 | 0.14 | 0.047960 | 0.12 | 0.448 | 2.275 | 94.133 | 0.04 | 94.133 | 0.12 | 96.2 | 2.9 |
| z8 | 33.31 | 63.79 | 0.52 | 0.58 | 3806 | 0.014664 | 0.13 | 0.096891 | 0.17 | 0.047986 | 0.10 | 0.792 | 3.843 | 93.846 | 0.12 | 93.902 | 0.15 | 97.5 | 2.4 |
| z9 | 9.68 | 18.84 | 0.51 | 0.77 | 1084 | 0.014756 | 0.04 | 0.097283 | 0.32 | 0.047878 | 0.31 | 0.273 | −2.355 | 94.426 | 0.04 | 94.265 | 0.29 | 92.2 | 7.4 |
| CT103 | | | | | | | | | | | | | | | | | | | |
| z1 | 116.61 | 191.44 | 0.61 | 0.07 | 12 326 | 0.207141 | 0.07 | 3.227135 | 0.13 | 0.113053 | 0.08 | 0.771 | 34.344 | 1213.6 | 0.8 | 1463.7 | 1.0 | 1848.2 | 1.6 |
| z2 | 1.25 | 2.23 | 0.56 | 0.65 | 147 | 0.014757 | 0.45 | 0.095685 | 4.66 | 0.047088 | 4.57 | 0.253 | −79.302 | 94.437 | 0.43 | 92.8 | 4.1 | 53 | 109 |
| z4 | 1.35 | 4.15 | 0.33 | 0.77 | 252 | 0.014769 | 0.26 | 0.094101 | 2.78 | 0.046271 | 2.73 | 0.233 | −785.641 | 94.510 | 0.24 | 91.3 | 2.4 | 11 | 66 |
| z5 | 1.11 | 1.41 | 0.79 | 0.64 | 100 | 0.014736 | 0.69 | 0.092917 | 7.66 | 0.045792 | 7.55 | 0.203 | 753.828 | 94.303 | 0.64 | 90.2 | 6.6 | −14 | 182 |
| z6 | 0.99 | 2.60 | 0.38 | 0.66 | 169 | 0.014793 | 0.44 | 0.100174 | 3.86 | 0.049178 | 3.80 | 0.177 | 39.078 | 94.665 | 0.41 | 96.9 | 3.6 | 155 | 89 |
| z8 | 0.61 | 1.64 | 0.37 | 0.66 | 113 | 0.014800 | 0.60 | 0.097716 | 6.37 | 0.047948 | 6.28 | 0.196 | 1.058 | 94.709 | 0.56 | 94.7 | 5.8 | 96 | 149 |
| HK017 | | | | | | | | | | | | | | | | | | | |
| _2_z1 | 5.28 | 7.70 | 0.69 | 0.47 | 487 | 0.014836 | 0.13 | 0.092947 | 1.51 | 0.045502 | 1.49 | 0.204 | 418.367 | 94.936 | 0.13 | 90.25 | 1.30 | −30 | 36 |
| _2_z3 | 1.44 | 1.36 | 1.06 | 0.60 | 98 | 0.014884 | 0.73 | 0.097087 | 7.60 | 0.047372 | 7.50 | 0.185 | −42.091 | 95.242 | 0.69 | 94.08 | 6.83 | 67 | 179 |
| _2_z6 | 4.76 | 2.07 | 2.30 | 0.52 | 142 | 0.014759 | 0.45 | 0.098241 | 4.65 | 0.048342 | 4.59 | 0.167 | 17.948 | 94.449 | 0.42 | 95.15 | 4.22 | 115 | 108 |
| z7 | 4.41 | 7.26 | 0.61 | 0.70 | 434 | 0.014743 | 0.15 | 0.097406 | 1.48 | 0.047982 | 1.46 | 0.212 | 3.156 | 94.343 | 0.14 | 94.38 | 1.33 | 97 | 34 |
| z8 | 3.56 | 7.52 | 0.47 | 0.61 | 459 | 0.014771 | 0.16 | 0.096433 | 1.47 | 0.047413 | 1.43 | 0.296 | −36.837 | 94.524 | 0.15 | 93.48 | 1.31 | 69 | 34 |
| z9 | 3.99 | 2.16 | 1.85 | 0.58 | 145 | 0.014761 | 0.48 | 0.098325 | 4.52 | 0.048378 | 4.46 | 0.177 | 19.170 | 94.457 | 0.45 | 95.23 | 4.11 | 117 | 105 |
| z10 | 7.44 | 4.70 | 1.58 | 0.62 | 292 | 0.014828 | 0.21 | 0.098615 | 2.13 | 0.048300 | 2.10 | 0.199 | 16.060 | 94.884 | 0.20 | 95.50 | 1.94 | 113 | 50 |
| z11 | 9.26 | 2.84 | 3.26 | 0.82 | 176 | 0.014761 | 0.36 | 0.097193 | 3.71 | 0.047816 | 3.67 | 0.179 | −5.927 | 94.459 | 0.34 | 94.18 | 3.34 | 89 | 87 |
| CT041 | | | | | | | | | | | | | | | | | | | |
| _1_z1 | 2.46 | 9.24 | 0.27 | 1.09 | 503 | 0.014868 | 0.11 | 0.097522 | 1.01 | 0.047626 | 0.96 | 0.568 | −19.361 | 95.141 | 0.10 | 94.486 | 0.92 | 79.7 | 22.7 |
| _1_z2A | 15.65 | 49.38 | 0.32 | 0.61 | 2925 | 0.014818 | 0.04 | 0.097927 | 0.16 | 0.047995 | 0.15 | 0.391 | 3.300 | 94.822 | 0.04 | 94.861 | 0.14 | 98.0 | 3.5 |
| _1_z3B | 6.95 | 10.06 | 0.69 | 0.86 | 575 | 0.014785 | 0.10 | 0.097697 | 0.56 | 0.047984 | 0.51 | 0.583 | 2.937 | 94.614 | 0.09 | 94.648 | 0.51 | 97.4 | 12.2 |
| _1_z6 | 20.27 | 54.64 | 0.37 | 0.71 | 3159 | 0.014782 | 0.04 | 0.097667 | 0.13 | 0.047982 | 0.11 | 0.452 | 2.871 | 94.594 | 0.03 | 94.620 | 0.11 | 97.3 | 2.7 |
| _2_z1A | 3.83 | 8.51 | 0.45 | 0.80 | 497 | 0.014766 | 0.14 | 0.097309 | 0.70 | 0.047857 | 0.65 | 0.446 | −3.598 | 94.491 | 0.13 | 94.289 | 0.63 | 91.1 | 15.4 |
| AD175 | | | | | | | | | | | | | | | | | | | |
| _1_z1 | 5.64 | 15.14 | 0.37 | 0.56 | 921 | 0.014914 | 0.06 | 0.098479 | 0.38 | 0.047955 | 0.35 | 0.484 | 0.691 | 95.432 | 0.05 | 95.372 | 0.35 | 93.9 | 8.4 |
| _1_z2 | 13.06 | 18.02 | 0.72 | 0.75 | 1044 | 0.014882 | 0.36 | 0.097749 | 0.55 | 0.047699 | 0.40 | 0.674 | −14.249 | 95.229 | 0.34 | 94.696 | 0.49 | 81.3 | 9.6 |
| _1_z5A | 61.28 | 29.56 | 2.07 | 0.42 | 1849 | 0.014879 | 0.17 | 0.098374 | 0.25 | 0.048020 | 0.17 | 0.704 | 4.097 | 95.210 | 0.16 | 95.275 | 0.23 | 96.9 | 4.2 |
| _1_z5C | 18.08 | 30.05 | 0.60 | 0.40 | 1889 | 0.014863 | 0.06 | 0.098327 | 0.20 | 0.048049 | 0.18 | 0.476 | 5.582 | 95.108 | 0.05 | 95.231 | 0.18 | 98.3 | 4.3 |
| _2_z1 | 57.30 | 16.08 | 3.56 | 0.41 | 1018 | 0.014831 | 0.25 | 0.097969 | 0.41 | 0.047979 | 0.29 | 0.701 | 2.417 | 94.902 | 0.23 | 94.900 | 0.37 | 94.8 | 6.9 |
| _2_z2 | 44.75 | 42.06 | 1.06 | 0.38 | 2648 | 0.014881 | 0.27 | 0.098346 | 0.32 | 0.048001 | 0.14 | 0.902 | 3.189 | 95.221 | 0.26 | 95.248 | 0.29 | 95.9 | 3.3 |
| z3 | 5.42 | 5.29 | 1.02 | 0.92 | 307 | 0.015084 | 1.19 | 0.098845 | 1.78 | 0.047583 | 1.24 | 0.722 | −24.436 | 96.514 | 1.14 | 95.710 | 1.63 | 75.7 | 29.4 |
| z4a | 8.28 | 7.11 | 1.16 | 0.87 | 411 | 0.014972 | 0.40 | 0.098264 | 1.11 | 0.047660 | 1.00 | 0.433 | −17.647 | 95.798 | 0.38 | 95.172 | 1.01 | 79.5 | 23.8 |

[a] Total mass of radiogenic Pb.
[b] Ratio of radiogenic Pb (including $^{208}Pb$) to common Pb.
[c] Total mass of common Pb.
[d] Th contents calculated from radiogenic $^{208}Pb$ and the $^{207}Pb/^{206}Pb$ date of the sample, assuming concordance between U–Th and Pb systems.
[e] Measured ratio corrected for fractionation and spike contribution only.
[f] Measured ratios corrected for fractionation, tracer and blank.
[g] Corrected for initial Th/U disequilibrium using radiogenic $^{208}Pb$ and Th/U[magma] = 2.80000.
[h] % discordance = 100 − (100* ($^{206}Pb/^{238}U$ date)/($^{207}Pb/^{206}Pb$ date)).
[i] Isotopic dates calculated using the decay constants λ238 = 1. 55125E−10 and λ235 = 9. 8485E−10 (Jaffey et al., 1971).

**Table 1b**
U–Pb Zircon CA-ID-TIMS summary data for volcanic tuff horizons throughout the CTBI, Yezo Group, Japan.

| Sample ID | $^{206}Pb/^{238}U$ date (Ma) | ±[a] | ±[b] | MSWD | dates used |
|---|---|---|---|---|---|
| HK018 | 93.920 | 0.031 | 0.11 | 2.0 | youngest 3 (of 13) |
| CT103 | 94.536 | 0.170 | 0.21 | 0.4 | youngest 6 (of 6) |
| HK017 | 94.436 | 0.093 | 0.14 | 0.8 | youngest 5 (of 8) |
| CT041 | 94.591 | 0.031 | 0.11 | 1.3 | youngest 3 (of 5) |
| AD175 | 95.114 | 0.048 | 0.12 | 1.5 | youngest 5 (of 8) |

[a] Analytical.
[b] Analytical + tracer + $^{238}U$ decay constant.

Du Vivier et al., 2014). In the YG the $^{192}Os$ concentration increases from ~5 ppt to 90 ppt over ~1 m interval, and within a 20 m interval returns to ~14 ppt. In the GVS the $^{192}Os$ values are variable (~3.6 to 172.7 ppt), but mostly fall between ~4 and 23 ppt. No appreciable shift in $^{192}Os$ concentrations is identified in the GVS except at ~72 m, which occurs between point A and B of the $\delta^{13}C_{wood}$ record in the OAE 2 interval, where the $Os_i$ value is unradiogenic (Fig. 2; discussed below). Although the $^{192}Os$ abundances are low (majority 4–23 ppt; Supplementary Tables 1a, 1b) in both the YG and GVS sections compared to other OAE 2 sections, the $^{192}Os$ values are similar to Furlo and Vocontian Basin. The latter both yield globally representative $Os_i$ profiles (Turgeon and Creaser, 2008; Du Vivier et al., 2014).

### 4.2. $Os_i$ stratigraphy of the Yezo Group, Japan

The $Os_i$ values for the YG show similar features to other OAE 2 sections, but especially the WIS (Du Vivier et al., 2014; Fig. 2 and supplementary material Table 1a). For the YG the $Os_i$ are radiogenic and moderately heterogeneous (0.66–0.80) from −130 m to −17 m. A brief and abrupt trend to a less radiogenic value of 0.52 is recorded at −63 m, before returning to radiogenic values (Fig. 2). The $Os_i$ data rapidly become unradiogenic at −16.1 m from 0.69 to 0.19, this is characteristic of all $Os_i$ profiles for the OAE 2 (Turgeon and Creaser, 2008; Du Vivier et al., 2014). The $Os_i$ values remain unradiogenic for ~20 m, before they abruptly return to radiogenic $Os_i$ (0.50) at ~7 m (Fig. 2). For the remainder of OAE 2 and post-dating the event, the $Os_i$ values are radiogenic and relatively homogeneous, 0.50–0.63 (Fig. 2).

### 4.3. $Os_i$ stratigraphy of the Great Valley Sequence, USA

The $Os_i$ values for the GVS show similar and distinct characteristics to the YG and other OAE 2 sections (Fig. 2; Supplementary Material Table 1b; Du Vivier et al., 2014). Key similarities are: 1) the distinct trend to non-radiogenic $Os_i$ from 0.38 at 40.4 m to 0.13 at 49.5 m, the OAE 2 onset interval; 2) an interval of predominantly non-radiogenic $Os_i$ compositions from 49.5 m to 78.9 m (datum levels A to B of the $\delta^{13}C_{wood}$ record); and 3) a progressive increase to more radiogenic $Os_i$ (~0.2 to 0.7) after datum level B of the $\delta^{13}C_{wood}$ record. Distinct differences in the $Os_i$ data of the GVS are; 1) the single point radiogenic (0.79–0.95) to non-radiogenic profile (0.32–0.40) of the pre-OAE 2 section (0–34.5 m), and 2) the presence of slightly more radiogenic $Os_i$ (0.3–0.7) among the predominantly non-radiogenic (~0.2) during the initial stages of the OAE 2 (datum levels A to B of the $\delta^{13}C_{wood}$ record).

As noted above the $^{192}Os$ for the GVS are consistently low (~4 to 23 ppt; and lower than the continental average, ~50 ppt), especially for the pre-OAE 2 and initial stages of the OAE 2 intervals. Regardless of the low $^{192}Os$ abundances, the interval between 40.4 m and 49.5 m shows the overall same $Os_i$ trend as all other global OAE 2 sections, and thus trace the change in the contemporaneous seawater $^{187}Os/^{188}Os$ composition. The pre OAE interval below 40.4 m comprises similar stratigraphy to that above it, with no evidence of post-deposition disturbance to the Re–Os systematics (weathering, veining, faulting), and exhibits low $^{192}Os$, however shows a single point unradiogenic/radiogenic $Os_i$ profile. If the stratigraphy between 40.4 m and 49.5 m records the seawater $^{187}Os/^{188}Os$ of the GVS palaeobasin, we therefore also interpret the $Os_i$ of the entire pre-OAE 2 interval to record the $^{187}Os/^{188}Os$ of the water column (see discussion and Supplemental Material).

### 4.4. $^{206}Pb/^{238}U$ zircon geochronology and stratigraphic age-model

For each volcanic tuff sample we identify the population of youngest concordant zircon U–Pb analyses and calculate a $^{206}Pb/^{238}U$ weighted mean age as an approximation for the eruption age of the ash layer (Tables 1a, 1b; Fig. 3). The coherence of the youngest population is assessed via the MSWD value, each of which is within the acceptable range for the given number of analyses (Wendt and Carl, 1991). In each case the mean age is based on three to five individual $^{206}Pb/^{238}U$ dates that include the youngest $^{206}Pb/^{238}U$ date in each sample. The assumption made here is that zircon was crystallising in the magma chamber immediately prior to eruption such that the youngest zircons/zircon domains will yield $^{206}Pb/^{238}U$ dates that approximate the eruption age, and inferentially the absolute age of the stratigraphic level sampled. Older $^{206}Pb/^{238}U$ (zircon) dates are interpreted as reflecting crystallisation in a magmatic system prior to eruption and/or the inclusion of older materials during explosive volcanism and/or ash deposition. Alternative ways to interpret the distribution of $^{206}Pb/^{238}U$ dates from an ash bed are possible (see supplementary material). We chose a 'youngest coherent' population of $^{206}Pb/^{238}U$ dates as considered to best approximate the time elapsed since eruption and deposition, having considered the potential for minor Pb-loss and mitigation via pretreatment methods employed (Mattinson, 2005), inheritance and recycling. We report preferred $^{206}Pb/^{238}U$ weighted mean ages of 95.114 ± 0.048/0.12 Ma (AD175), 94.591 ± 0.031/0.11 Ma (CT041), 94.436 ± 0.093/0.14 Ma (HK017), 94.530 ± 0.170/0.21 Ma (CT103) and 93.920 ± 0.031/0.11 Ma (HK018) with MSWD values ranging between 0.4 to 2.0 (Fig. 3; Table 1b), values that are acceptable for a single population of the given sample size (Wendt and Carl, 1991). The uncertainties reflect the following sources: analytical/(analytical + tracer solution calibration + $^{238}U$ decay constant); the latter value is the total uncertainty in each case which should be used when comparing these dates to other non-U–Pb derived dates (i.e., the age model for the CTB from Meyers et al., 2012a that are largely based upon $^{40}Ar/^{39}Ar$ data), the former is to be used when quantifying differences between dates in this study.

We generate age–depth models using OxCal (Bronk Ramsey, 2008) through a combination of likelihood estimates (radioisotopic dates and uncertainties from ash beds), prior information (sediment thickness) using the *P sequence* depositional model where deposition is assumed to be random giving approximate proportionality to depth (Bronk Ramsey, 2008; Fig. 4; supplementary material Tables 3a, 3b and 3c). The age–depth model illustrates the temporal relationships of the tuff horizons relative to depth and permits the interpolation of ages between the dated tuff horizons for the YG section, and thus facilitates objective comparison of the YG and WIS sections based on the stratigraphy, $\delta^{13}C$ and the $Os_i$ profiles they contain.

For the YG section the $^{206}Pb/^{238}U$ zircon dates, with the exception of CT103 (94.53 ± 0.21 Ma), conform to stratigraphic order (Figs. 2, 3, 4), however the age model forces superposition to be upheld and derives a new interpolated age for that level (Fig. 4 – dark grey area of sample). For CT103 it is likely that the zircons either record inheritance and/or crystallisation in the magmatic chamber a period of time prior to eruption since the sample yields

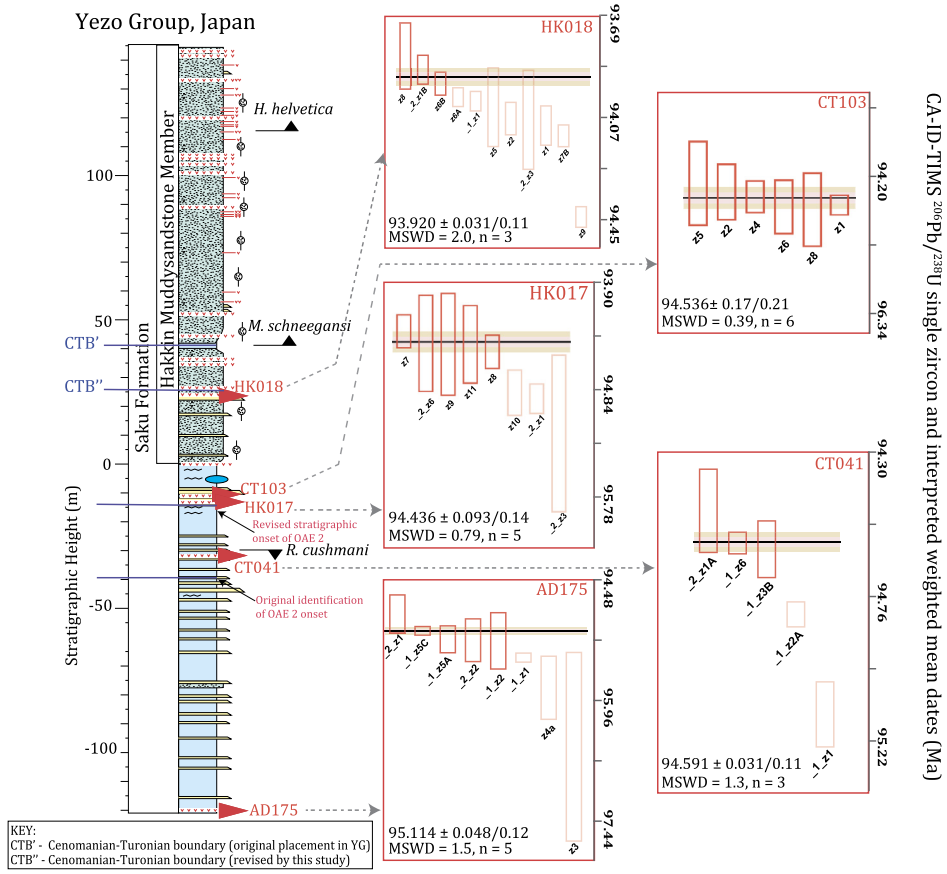


**Fig. 3.** Lithostratigraphy and biostratigraphy of the Yezo Group section, Japan with CA-ID-TIMS $^{206}Pb/^{238}U$ single zircon and interpreted weighted mean ages. $^{206}Pb/^{238}U$ weighted mean ages, bold red squares, are plotted with analytical uncertainties ($2\sigma$) and with total uncertainties ($2\sigma$). Analyses excluded from weighted mean calculation for $^{206}Pb/^{238}U$ (i.e., Pb loss; inheritance) are indicated by opaque red squares (see text for discussion). The MSWD and the number of single zircon analyses included for each sample are also shown (see text for discussion, Wendt and Carl, 1991).

a date older than zircons from tuff units below CT103, e.g., HK017 ($94.44 \pm 0.093$ Ma).

The published WIS temporal framework is based on an integrated approach, which combines $^{206}Pb/^{238}U$ (zircon) and $^{40}Ar/^{39}Ar$ (sanidine) radio-isotopic data with astrochronology using Markov Chain Monte Carlo simulations (Meyers et al., 2012a). The accuracy of these radio-isotopic dates are based upon their respective calibrations, the age of the Fish Canyon sanidine (FCs) at 28.201 Ma for the $^{40}Ar/^{39}Ar$ dates, the gravimetric calibration of the EARTHTIME mixed U–Pb tracer for the zircon U–Pb dates, and the interpretation of the mineral dates as reflecting both eruption and deposition ages. Although there is potential for bias between the geochronological systems, particularly related to the choice of an age of 28.201 Ma for FCs, a suite of new $^{206}Pb/^{238}U$ (zircon) and $^{40}Ar/^{39}Ar$ (sanidine) data for the Cretaceous Niobara Formation in the WIS suggest no resolvable bias (Sageman et al., 2014). It is worth noting that the WIS age model (Meyers et al., 2012a) is based upon a number of radio-isotopic dates from outcrops across the WIS (i.e., Arizona, Nebraska, New Mexico and Colorado). These dates have been imported into the Portland #1 core stratigraphy (Meyers et al., 2012a) using biostratigraphic correlation with no additional uncertainty included for Arizona, Nebraska, New Mexico ash beds to account for uncertainty contribution related to inter-regional correlation. In contrast the Colorado ash beds can be placed with the Portland #1 core section using bed by bed correlations with minimal uncertainty contribution. The integrated chronostratigraphy of the CTBI based on Meyers et al. (2012a) derived age model for the Portland #1 core, coupled with a linear sedimentation rate has been previously used to derive a nominal age for the onset of OAE 2 at $\sim 94.38 \pm 0.15$ Ma (Du Vivier et al., 2014).

When comparing age models for the YG and WIS CTBI sections, the accuracy and direct comparison of the temporal constraints is paramount. Thus we select only a subset of the $^{40}Ar/^{39}Ar$ data for the WIS for age construction, giving preference to those that can be directly correlated with ash beds that occur in the Portland record (i.e., samples K-07-01C and K-07-01B from the GSSP type locality), in order to reduce additional (or unrecognised) uncertainties associated with biostratigraphic correlation including a known hiatus (Fig. 4; Ma et al., 2014; see Sageman et al., 2014 for further discussion). In order to justify using the $^{40}Ar/^{39}Ar$ dates we tested an age–depth model based on $^{40}Ar/^{39}Ar$ ages and astronomical tuning (Meyers et al., 2012a; Ma et al., 2014), which showed no discernible variation within uncertainty to the model used in this study (Fig. 4; Supplementary Fig. S1). The youngest date used, labelled "Meyers C" in the figures is the age of the K-07-01C sample in Meyers et al. (2012a). The age labelled "Meyers B" is the age of the K-07-01B sample in Meyers et al. (2012a). The age labelled "Meyers A" is the combined mean age given for "Tuff A" in Meyers et al. (2012a) based on samples AZLP-08-02 and 90-O-31 from Lohali Point, Arizona, as there is no date available from the Colorado sections/cores. The oldest age used in the models is the age published for the *Dunveganoceras pondi* Zone core (Ma et al., 2014). The *D. pondi* Zone occurs in the WIS as the uppermost ammonite zone of the Lincoln Limestone, beneath the Hartland shale (Adams et al., 2010; Ma et al., 2014). In the Portland core the *D. pondi* Zone is ~4 metres thick (Joo et al., in press), from metre level −20 to −16 in our age–depth model. As such the *D. pondi* $^{40}Ar/^{39}Ar$ date (Ma et al., 2014) is placed at metre level −18 (see Supplemental material for further detail).

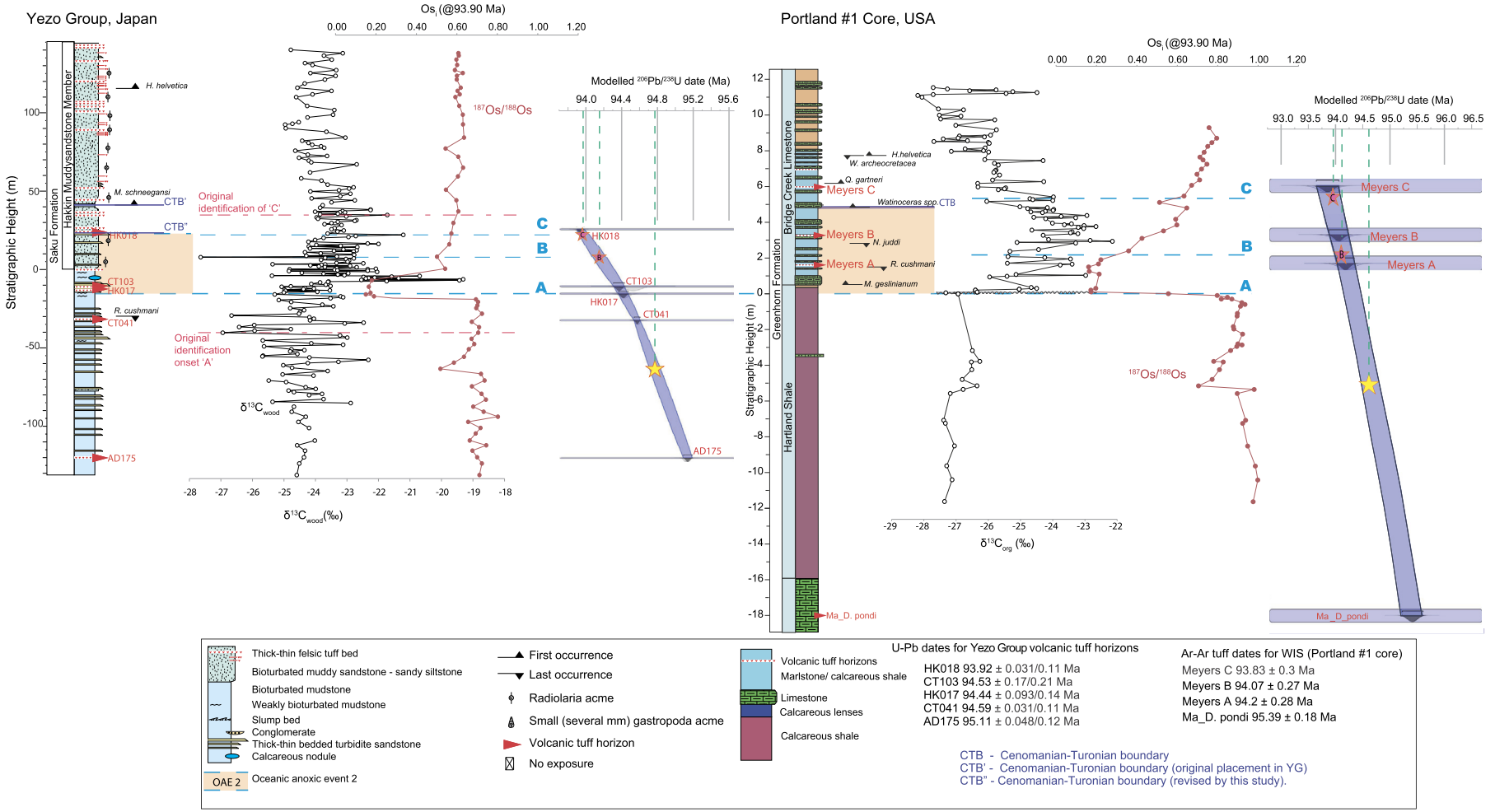


**Fig. 4.** Lithostratigraphy and Tuff ID of the Yezo Group section and Portland #1 core vs. Chemostratigraphy of the Yezo Group section and Portland # 1 core vs. the OxCal age-models. The light grey areas represent the distribution for single calibrated dates. The dark grey areas demonstrate the marginal posterior distribution (Bronk Ramsey, 2008; see text for discussion; supplementary material Table 3). The $\delta^{13}C_{wood}$ and $\delta^{13}C_{org}$ (black) and $Os_i$ (red) profiles are plotted against stratigraphic height. $^{206}Pb/^{238}U$ and $^{40}Ar/^{39}Ar$ weighted mean ages are given with total uncertainties ($2\sigma$; analytical + tracer + $^{238}U$ decay constant) and the age of the CTB $93.90 \pm 0.07/0.15$ Ma is from Meyers et al. (2012a). Ages between dated tuff horizons can be interpolated from both the WIS and the Yezo Group, which can be projected on to the isotope profiles of the Portland core and the Yezo Group section, respectively (see text for discussion). Equally, stratigraphic datum levels (pink stars 'B' and 'C') or isotope values (yellow star) can be projected on to the age-model to clarify trans-basin integration (see text for discussion). The stratigraphic thickness of the OAE 2 interval (shaded) reflects a variation of the chemostratigraphic approach defining widely recognised elements of the C isotope excursion (A, B, and C datum levels).

## 5. Discussion

### 5.1. Global chronology of OAE 2 events, synchroneity and CTB

Traditionally the OAE 2 onset is identified by a positive excursion in the $\delta^{13}C$ record (datum level 'A', Pratt et al., 1985; Schlanger et al., 1987; Jenkyns, 1980) and the whole OAE 2 sequence is correlated through datum levels 'A', 'B' and 'C'. Coincident with the positive $\delta^{13}C$ excursion, datum level 'A', $Os_i$ profiles for all previously studied Atlantic, WIS and European pelagic shelf OAE 2 sections exhibit an abrupt shift from radiogenic (~0.7 to 1.0) to unradiogenic values (~0.20 to 0.30; Fig. 5; Turgeon and Creaser, 2008; Du Vivier et al., 2014). This trend is interpreted as a signal of LIP-related submarine volcanism (Turgeon and Creaser, 2008; Du Vivier et al., 2014). Both the High Arctic and Caribbean LIP had major eruptions close to the time of the CTBI (Snow et al., 2005; Tegner et al., 2011; Fig. 1). Whole rock total fusion Ar–Ar ages of the Dumisseau Formation, Haiti, of the Caribbean LIP show the most temporal relationship with the onset of the OAE 2 (mean of $94.57 \pm 0.38$ Ma ($n = 4$) adjusted using the 0.65% correction based on the discrepancy between U–Pb and Ar–Ar dates; Snow et al., 2005; Kuiper et al., 2008).

In the YG the abrupt shift to unradiogenic $Os_i$ is ~23 m above the current identified key datum level, 'A', based on the averaged $\delta^{13}C_{wood}$ record (Takashima et al., 2011; Fig. 2). Tuff unit HK017 in the YG section occurs at −16.10 m, above the first least radiogenic $Os_i$ value. The U–Pb zircon systematics for tuff HK017 yield a date of $94.44 \pm 0.14$ Ma, which is indistinguishable within uncertainty for the first least radiogenic $Os_i$ in the WIS determined by the age–depth model ($94.28 \pm 0.25$ Ma; Fig. 4). This age is identical within uncertainty, to a previous estimate ($\sim 94.38 \pm 0.15$ Ma) obtained from astrochronology and radio-isotopic dating in the WIS (Meyers et al., 2012a) that were used to establish a chronostratigraphic framework (Du Vivier et al., 2014). Further, additional litho- and biostratigraphy (Takashima, pers. comm.) combined with the unradiogenic $Os_i$ for the YG is consistent with the onset of the OAE 2 in all sections previously studied (Turgeon and Creaser, 2008; Du Vivier et al., 2014). Therefore, given the temporal agreement of the first least radiogenic $Os_i$ in both the YG and WIS sections, plus the coincidence of both $Os_i$ and $\delta^{13}C_{org}$ excursions in the WIS, Atlantic and European OAE 2 sections we propose that the onset of the OAE 2 in YG section has been misidentified and should be placed at $\sim -16.1$ m. At this interval the $\delta^{13}C_{wood}$ record starts to shift to heavier values and coincides with a sudden increase in the degree of pyritization (Supplementary Material Table 4 and Fig. S3; Takashima et al., 2011). The shift to heavier $\delta^{13}C$ values up to the first peak occurs ≤10 m above the first unradiogenic $Os_i$ value. Based on the 5 point moving average of the $\delta^{13}C$ record (Takashima et al., 2011), it is worth noting that the $\delta^{13}C$ excursion may occur over a shorter duration. Therefore absolute time constraints on chemostratigraphy are necessary, i.e., the U–Pb zircon dates, which remove the uncertainty between correlating varying isotopic proxies and quantitatively constrain events in stratigraphy. Thus the increase in $\delta^{13}C$ at the onset of the OAE 2 is contemporaneous with an enhanced unradiogenic Os flux to the ocean associated with volcanism, which is a globally isochronous event at ~94.4 Ma (Figs. 2, 4, 5). Therefore the $Os_i$ profile can be adopted as a surrogate proxy to identify the onset of OAE 2.

The CTB cannot be placed accurately in the YG section using the available biostratigraphy; therefore we propose using the age–depth model to place the CTB. The age of tuff HK018, $93.92 \pm 0.03/0.11$ Ma from the YG, implies that the CTB (dated at $93.90 \pm 0.15$ Ma, WIS; Meyers et al., 2012a) in the YG is present in the horizon directly above or below the tuff since the date for HK018 is statistically indistinguishable from the date of the numerical age of the CTB (derived from the WIS). As such we amend the stratigraphic height of the CTB in the YG to ~25 m. In addition, the age–depth models and $Os_i$ data allow us to quantitatively import the datum levels B and C derived from the global $\delta^{13}C$ record (Fig. 4 pink stars 'B' and 'C').

The application of age–depth models, in addition to integrating the onset of OAE 2 and the CTB between the YG and WIS (Section 5.1), provide absolute age constraints for the datum levels ('A', 'B', 'C') assigned to peaks and troughs on the $\delta^{13}C$ records, which can be used to correlate the $Os_i$ chemostratigraphy within uncertainty from other trans-basin sections. Unlike the YG and WIS the GVS has no means of defining absolute time, therefore for the GVS, as for other locations bereft of geochronology, we apply a chronostratigraphic framework relative to individual timescales created for each section (Du Vivier et al., 2014), exporting numerical information based on integrated radio-isotope dates (U–Pb and Ar–Ar; Meyers et al., 2012a; Ma et al., 2014) and astrochronology (Meyers et al., 2012a). The dates are used to constrain the linear sedimentation rate values (cm/kyr) for the units between the datum levels (Supplementary Material Table 5) and thus derive an age model in order to quantitatively assess the duration of events occurring across the CTBI based on the $Os_i$ profile (Fig. 6). The temporal uncertainty for these datum levels is ≤0.25 Myr. For the GVS we apply the temporal model based on the numerical ages of the datum levels derived from the age–depth model for the YG section. The framework utilises the onset of OAE 2 as datum level 'A', which is set to 0 kyrs, based on the revised onset of OAE 2 determined in this study (Figs. 2, 6; Section 5.1). Presenting the $Os_i$ profiles on the temporal framework further supports the revised onset of OAE 2 and the adjustment of the CTB in the YG determined from U–Pb geochronology and age–depth models (Sections 4.4 and 5.1). In addition, analyses of the degree of pyritization, as noted in the YG, records a temporal synchronous increase at the OAE 2 onset (Supplementary Material Table 4 and Fig. S3; Takashima et al., 2011). Moreover, the framework can potentially reduce the discrepancy observed in stratigraphic correlations based solely on $\delta^{13}C$ records.

The temporal framework for the GVS illustrates that the $Os_i$ data for the pre-OAE 2 interval between ~350 and 80 kyr prior to the OAE 2 onset is different in comparison to that of WIS, and Japan, and other OAE 2 sites (Fig. 6; Fig. 5 Du Vivier et al., 2014). The GVS shows, at an interval of ~20–30 kyr, single point unradiogenic/radiogenic shifts between ~350 and 80 kyr before the onset of OAE 2. The implications of the pre-OAE 2 GVS profile are discussed below.

### 5.2. Implications of the $Os_i$ radiogenic pre-OAE 2 trend in YG, WIS and GVS

For both the YG and WIS sites between ~94.7 and 94.4 Ma $Os_i$ values become markedly radiogenic (Fig. 4). However, in the same time interval, for ODP Site 1260 (Demerera Rise) the $Os_i$ profile trends steadily to more unradiogenic values (Fig. 5; Turgeon and Creaser, 2008; Du Vivier et al., 2014). For the WIS Du Vivier et al. (2014) proposed the contrast in $Os_i$ values was related to the degree of connectivity of the WIS with the open ocean and that Site 1260 recorded a more open-ocean signal. Radiogenic $Os_i$ values are interpreted to reflect weathering of the continental crust (Peucker-Ehrenbrink and Ravizza, 2000; Cohen, 2004). As such the $Os_i$ values at YG and WIS must be controlled by radiogenic influx in comparison to Site 1260, which reflects a progressive incorporation of unradiogenic Os sourced from LIP activity (Du Vivier et al., 2014). Encompassing the same time interval, unradiogenic $Os_i$ values are also recorded in the GVS in addition to single shifts to radiogenic $Os_i$ values (Fig. 6). We consider the GVS $Os_i$ record up to 80 kyr prior to the OAE 2 to record either a pulsed LIP activity and/or alternating sea level and accelerated weathering. Given the $Os_i$ profile of site 1260 and that sea level change is characteristic

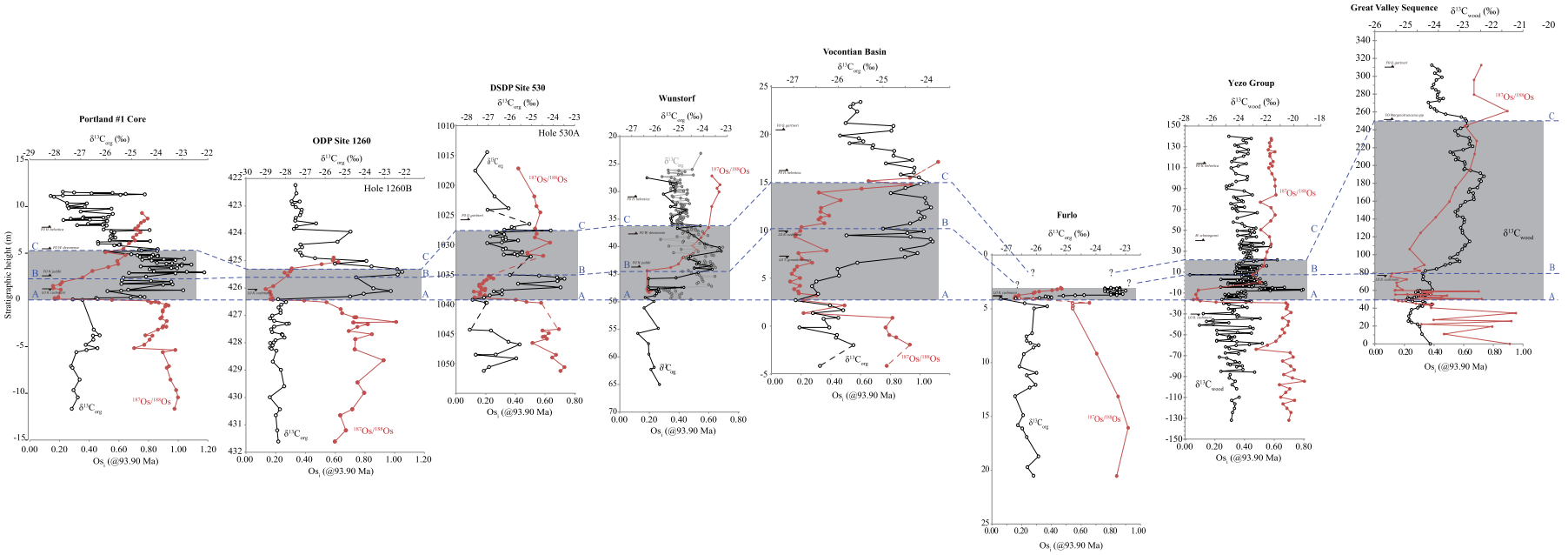


**Fig. 5.** Global correlation of $\delta^{13}C_{org}$ and $\delta^{13}C_{wood}$ (black) and $Os_i$ (red) vs. stratigraphic height (m). Initial $^{187}Os/^{188}Os$ calculated at 93.90 ± 0.15 Ma. $\delta^{13}C$ data from: Portland # 1 Core, Sageman et al. (2006); Site 1260, Forster et al. (2007); Wunstorf, Du Vivier et al. (2014); Vocontian Basin, Jarvis et al. (2011); Furlo, Jenkyns et al. (2007); Site 530, Forster et al. (2008); Yezo Group, Takashima et al. (2010); Great Valley Sequence, Takashima et al. (2010). Sites correlated using datum levels on the $\delta^{13}C$ record (A, B, C; see text for details), 'A' denotes the onset of the OAE 2. Grey shaded area marks the OAE 2 interval defined by the elements of the C isotope excursion (A, B, and C datum levels). Biostratigraphic horizons are labelled: FO – first occurrence, LO – last occurrence. The biozones illustrate low resolution and inconsistent global distribution, which hampers correlation. Dashed lines represent intervals of pore core recovery. Note that symbol size is greater than the measured uncertainty. Osmium isotope data are reported for YG and GVS in supplementary material Tables 1a and 1b.

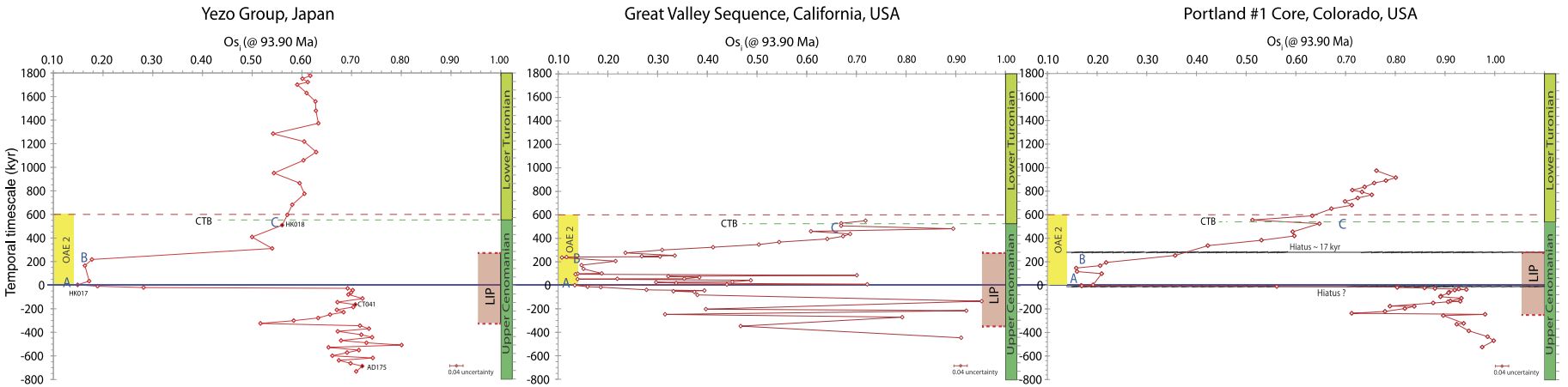


**Fig. 6.** $Os_i$ vs. temporal timescale (kyr). 'A', 'B' and 'C' represent the $\delta^{13}C$ correlative datum levels. The onset ('A') of OAE 2 is in blue and the Cenomanian–Turonian boundary (CTB) is in green. The duration of the OAE 2 is in yellow (~600 kyr; Meyers et al., 2012b). The tuff horizons in the Yezo Group are labelled and the adjacent $Os_i$ data point filled in black. The duration of LIP activity is in shaded pink (~600 kyr); derived from Du Vivier et al. (2014) and this study (see text for discussion). The 2 minor hiatuses in the Portland #1 core are marked on as black hashes. The uncertainty of each analysis is <0.04.

of the late Cenomanian and early Turonian (Haq et al., 1988; Erbacher et al., 1996; Jones and Jenkyns, 2001; Leckie et al., 2002; Forster et al., 2007) we suggest that the pre-OAE 2 GVS $Os_i$ data to record variable connectivity to the open ocean. The CTB global sea levels fluctuated approaching a highstand during the early Turonian (Haq et al., 1988; Erbacher et al., 1996). Following the pre-OAE 2, ≤80 kyr (≤95.2 Ma) prior to OAE 2 onset, all $Os_i$ profiles trend to unradiogenic $Os_i$, reaching the nadir at the OAE 2 onset (~94.4 Ma). The latter is concurrent with rising global sea level (Erbacher et al., 1996; Leckie et al., 2002) that permitted a global contemporaneous distribution of seawater chemistry, coincident with the OAE 2 onset as evident from Os isotopes (Fig. 5).

In addition to Os, Nd isotopes also assess water mass exchange and ocean circulation, whereby the $\epsilon_{Nd}$ record exhibits a positive excursion at the onset of OAE 2 at Demerara Rise and in the European pelagic shelf (MacLeod et al., 2008; Zheng et al., 2013), which implies a change in the source of circulation and input to the ocean (i.e., hydrothermal processes associated with LIP: MacLeod et al., 2008; Martin et al., 2012). Therefore a vigorous deep ocean circulation throughout the late Cretaceous combined with transgression permitted the exchange of Pacific seawater into the Atlantic, WIS and European pelagic basins across the CTB (Trabucho-Alexandre et al., 2010; Martin et al., 2012), which reflects the concurrent emplacement of the LIPs with the global $Os_i$ record (Fig. 5; Du Vivier et al., 2014).

### 5.3. Large igneous province activity throughout OAE 2 and CTBI

The unradiogenic $Os_i$ values across the OAE 2 interval reflects contemporaneous Os sourced from LIP activity (Turgeon and Creaser, 2008; Du Vivier et al., 2014). The utilisation of the age–depth models permits an improvement to the quantitative integration of WIS and YG sections. The age-model coupled with the $Os_i$ data permits an evaluation of the onset and duration of LIP activity throughout OAE 2. In the YG the unradiogenic $Os_i$ values and the return to radiogenic $Os_i$ values represents the timing of the onset and cessation of activity at $94.78 \pm 0.12$ Ma and $94.24 \pm 0.13$ Ma, respectively (Fig. 4). These dates are identical within uncertainty to those determined for the WIS ($94.66 \pm 0.25$ Ma and $94.02 \pm 0.25$ Ma, respectively; Fig. 4), and for the onset at Site 1260 ($94.56 \pm 0.25$ Ma; Du Vivier et al., 2014). For the GVS the first unradiogenic $Os_i$ in the pre-OAE 2 interval coincides with the timing established from YG, WIS, and Site 1260, at $94.75 \pm 0.25$ Ma. As for all OAE 2 sites, the GVS $Os_i$ values remain unradiogenic up to datum level 'B' when at ~240 kyr after the OAE 2 onset the $Os_i$ values become more radiogenic (Fig. 6) as the influence of volcanically derived Os decreased. The combined $Os_i$ data from four OAE 2 locations (YG, WIS, Site 1260 and GVS) suggests a revision to the duration of focused LIP activity during the CTBI from ~450 kyr (Du Vivier et al., 2014) to $600 \pm 0.15$ kyr, with the LIP activity beginning at ~350 kyr prior to the OAE 2 onset, and ceases at ~240 kyr after the onset coincident with datum level B of the $\delta^{13}C$ profile (Fig. 6).

## 6. Summary

The high-resolution $Os_i$ profiles for two proto-Pacific sections demonstrate the changes in global ocean chemistry across the OAE 2. The $Os_i$ stratigraphy augments the traditional method of correlation and integration of stratigraphic successions using $\delta^{13}C$ isotopes. In addition, we use the $^{206}Pb/^{238}U$ zircon ages to show the synchronous onset of OAE 2 and assess the duration of LIP activity. The use of U–Pb zircon dates (Fig. 3) has permitted the integration of $Os_i$ profiles from WIS and Pacific basins through the application of age–depth models (Fig. 4). We have revised the onset of OAE 2, the position of the CTB in the YG section, and confirmed the onset of OAE 2 in the GVS; all previously interpreted from $\delta^{13}C_{wood}$ record. Moreover, the application of a chronostratigraphic framework to both Pacific sections (Fig. 6) temporally supports the interpretations based on geochronology, and quantitatively constrain the duration of LIP activity ($\sim 0.6 \pm 0.15$ Myr). The improved integration of the proto-Pacific with the WIS across the CTB has created a nominal correlation to the GSSP in the WIS.

The YG and GVS sections are at the western and eastern periphery of the proto-Pacific ocean, respectively. The discrepancy between the $Os_i$ profiles further illustrates the extent of regional variability of inputs to basinal environments (Paquay and Ravizza, 2012). Overall the variability of the Os isotope composition throughout the CTBI is indicative of a dynamic palaeocirculation and fluctuating sea level, and highlights the sensitivity of the seawater chemistry in the GVS to regional basin inputs. Therefore circulation was not stagnant and was sufficient to re-equilibrate seawater chemistry of palaeobasins and peripheral margins of the oceans worldwide within the residence time of Os (Trabucho-Alexandre et al., 2010; Du Vivier et al., 2014).

Concatenating environmental conditions ultimately primed the ocean system for the development of anoxia. Despite the variability of the $Os_i$ values the overall trend of the $Os_i$ profiles: radiogenic – unradiogenic – return to radiogenic $Os_i$, are characteristic of the OAE 2 with respect to Os isotope stratigraphy throughout the proto-Atlantic, European pelagic shelf and WIS (Du Vivier et al., 2014). Therefore, with the addition of the high-resolution Os isotope stratigraphy from both proto-Pacific sections and new $^{206}Pb/^{238}U$ geochronology from the YG section, we conclude that the global Os isotope composition during OAE 2 was isochronous, reflecting global processes, but was overprinted in some locations by basin-scale processes.

## Acknowledgements

We would like to thank Nicola Atkinson and Diana Sahy for assistance with all the U–Pb chronology work at NIGL. The project was possible thanks to a grant for fieldwork in Japan awarded to A.D.C. Du Vivier by the Geological Society of London from the Timothy Jefferson Field Research Funds. This project was, in part, funded by a NERC standard grant (NE/H021868/1). A grant was awarded to Selby and Du Vivier from NIGFSC (NERC Isotope Geosciences Facilities Steering Committee) IP-1283-1111 for the U–Pb zircon geochronology of volcanic tuff horizons of the key palaeo-Pacific OAE 2 Yezo Group section, Japan. We thank Kathy Mather for her assistance in drafting the figures. Hugh Jenkyns, Brad Sageman, Steve Meyers, and two EPSL reviewers are thanked for their constructive comments.

## Appendix A. Supplementary material

Supplementary material related to this article can be found online at http://dx.doi.org/10.1016/j.epsl.2015.07.020.

## References

Adams, D.D., Hurtgen, M.T., Sageman, B.B., 2010. Volcanic triggering of biochemical cascade during Oceanic Anoxic Event 2. Nat. Geosci. 3. http://dx.doi.org/10.1038/NGEO743.

Arthur, M.A., Schlanger, S.O., Jenkyns, H.C., 1987. The Cenomanian/Turonian Oceanic Anoxic Event, II: palaeoceanographic controls on organic matter production and preservation. In: Brooks, J., Fleet, A.J. (Eds.), Marine Petroleum Source Rocks. In: Geol. Soc. (Lond) Spec. Publ., vol. 26, pp. 401–420.

Blättler, C.L., Jenkyns, H.C., Reynard, L.M., Henderson, G.M., 2011. Significant increases in global weathering during Oceanic Anoxic Events 1a and 2 indicated by calcium isotopes. Earth Planet. Sci. Lett. 309, 77–88.

Bronk Ramsey, C., 2008. Deposition models for chronological records. Quat. Sci. Rev. 27, 42–60.

Cohen, A.S., 2004. The rhenium–osmium isotope system: applications to geochronological and palaeoenvironmental problems. J. Geol. Soc. (Lond.) 161, 729–734.
Cohen, A.S., Coe, A.L., Bartlett, J.M., Hawkesworth, C.J., 1999. Precise Re–Os ages of organic-rich mudrocks and the Os isotope composition of Jurassic seawater. Earth Planet. Sci. Lett. 167, 159–173.
Condon, D.J., Schoene, B., McLean, N., Bowring, S.A., Parrish, R., 2015. Metrology and traceability of U–Pb isotope dilution geochronology (EARTHTIME Tracer Calibration Part I). Geochim. Cosmochim. Acta 164, 464–480. http://dx.doi.org/10.1016/j.gca.2015.05.026.
Du Vivier, A.D.C., Selby, D., Sageman, B.B., Jarvis, I., Grocke, D.R., Voigt, S., 2014. Marine $^{187}Os/^{188}Os$ isotope stratigraphy reveals the interaction of volcanism and ocean circulation during Oceanic Anoxic Event 2. Earth Planet. Sci. Lett. 389, 23–33.
Du Vivier, A.D.C., Jacobson, A.D., Lehn, G.O., Selby, D., Hurtgen, M.T., Sageman, B.B., 2015. Ca isotope stratigraphy across the Cenomanian–Turonian OAE 2: links between volcanism, seawater geochemistry, and the carbonate fractionation factor. Earth Planet. Sci. Lett. 416, 121–131.
Erbacher, J., Thurow, J., Littke, R., 1996. Evolution patterns of radiolaria and organic matter variations: a new approach to identify sea-level changes in mid-Cretaceous pelagic environments. Geology 24, 499–502.
Fernando, A.G.S., Nishi, H., Tanabe, K., Moriya, K., Iba, Y., Kodama, K., Murphy, M.A., Okada, H., 2011. Calcareous nannofossil biostratigraphic study of forearc basin sediments: lower to Upper Cretaceous Budden Canyon Formation (Great Valley Group). Isl. Arc 20, 346–370.
Forster, A., Schouten, S., Moriya, K., Wilson, P.A., Sinninghe Damsté, J.S., 2007. Tropical warming and intermittent cooling during the Cenomanian/Turonian oceanic anoxic event 2: sea surface temperature records from the equatorial Atlantic. Paleoceanography 22, PA1219. http://dx.doi.org/10.1029/2006PA001349.
Forster, A., Kuypers, M.M.M., Turgeon, S.C., Brumsack, H.-J., Petrizzo, M.R., Sinninghe Damste, J.S., 2008. The Cenomanian/Turonian oceanic anoxic event in the South Atlantic: new insights from a geochemical study of DSDP 530A. Palaeogeogr. Palaeoclimatol. Palaeoecol. 267, 256–283.
Haq, B.U., Hardenbol, J., Vail, P.A., 1988. Mesozoic and Cenozoic chronostratigraphy and cycles of sea-level change. In: Wilgus, C.K., et al. (Eds.), Sea-Level Changes: An Integrated Approach. In: Spec. Publ. Soc. Econ. Plaeontol. Mineral., vol. 42, pp. 71–108.
Hasegawa, T., 1995. Correlation of the Cenomanian/Turonian boundary between Japan and Western Interior of the United States. J. Geol. Soc. Jpn. 101, 2–12.
Hasegawa, T., 1999. Planktonic foraminifera and biochronology of the Cenomanian–Turonian (Cretaceous) sequence in the Oyubari area, Hokkaido, Japan. Paleontol. Res. 3, 173–192.
Hasegawa, T., Saito, T., 1993. Global sychroneity of a positive carbon isotope excursion at the Cenomanian/Turonian boundary: validation by calcareous microfossil biostratigraphy of the Yezo Group, Hokkaido, Japan. Isl. Arc 2, 181–191.
Hiess, J., Condon, D.J., McLean, N., Noble, S.R., 2012. $^{238}U/^{235}U$ systematics in terrestrial uranium-bearing minerals. Science 335, 1610–1614.
Jaffey, A.H., Flynn, K.F., Glendenin, L.E., Bentley, W.C., Essling, A.M., 1971. Precision measurement of half-lives and specific activities of $^{235}U$ and $^{238}U$. Phys. Rev. C, Nucl. Phys. 4, 1889–1906.
Jarvis, I., Lignum, J.S., Grocke, D.R., Jenkyns, H.C., Pearce, M.A., 2011. Black shale deposition, atmospheric $CO_2$ drawdown, and cooling during the Cenomanian–Turonian Oceanic Anoxic Event. Paleoceanography 26, PA3201.
Jenkyns, H.C., 1980. Cretaceous anoxic events: from continents to oceans. J. Geol. Soc. (Lond.) 137, 171–188.
Jenkyns, H.C., 2010. Geochemistry of oceanic anoxia events. Geochem. Geophys. Geosyst. 11. http://dx.doi.org/10.1029/2009GC002788.
Jenkyns, H.C., Matthews, A., Tsikos, H., Erel, Y., 2007. Nitrate reduction, sulfate reduction, and sedimentary iron isotope evolution during the Cenomanian–Turonian oceanic anoxic event. Paleoceanography 22. http://dx.doi.org/10.1029/2006PA001355.
Jones, C.E., Jenkyns, H.C., 2001. Seawater strontium isotopes, oceanic anoxic events, and seafloor hydrothermal activity in the Jurassic and Cretaceous. Am. J. Sci. 301, 112–149.
Joo, Y.J., Sageman, B.B., Hurtgen, M.T., in press. Cenomanian to Campanian carbon isotope record from the Western Interior Basin. J. Sediment. Res.
Kaiho, K., Fujiwara, O., Motoyama, I., 1993. Mid-Cretaceous faunal turnover of intermediate-water benthic foraminifera in the northwestern Pacific Ocean margin. Mar. Micropaleontol. 23, 13.
Kendall, B.S., Creaser, R.A., Ross, G.M., Selby, D., 2004. Constraints on the timing of Marinoan "Snowball Earth" glaciation by $^{187}Re–^{187}Os$ dating of a Neoproterozoic, post-glacial black shale in Western Canada. Earth Planet. Sci. Lett. 222, 729–740.
Kendall, B., van Acken, D., Creaser, R.A., 2013. Depositional age of the early Paleoproterozoic Klipputs Member, Nelani Formation (Ghaap Group, Transvaal Supergroup, South Africa) and implications for low-level Re–Os geochronology and Paleoproterozoic global correlations. Precambrian Res. 237, 1–12. http://dx.doi.org/10.1016/j.precamres.2013.08.002.
Kuiper, K.F., Deino, A., Hilgen, F.J., Krijgsman, W., Renne, P.R., Wijbrans, J.R., 2008. Synchronizing rock clocks of Earth history. Science 320, 500–504. http://dx.doi.org/10.1126/science.1154339.
Kuroda, J., Tanimizu, M., Hori, R.S., Suzuki, K., Ogawa, N.O., Tejada, M.L., Ohkouchi, N., 2011. Lead isotopic record of Barremian–Aptian marine sediments: implications for large igneous provinces and the Aptian climatic crisis. Earth Planet. Sci. Lett. 307, 126–134.
Leckie, R.M., Bralower, T.J., Cashman, R., 2002. Oceanic anoxic events and plankton evolution: biotic response to tectonic forcing during the mid-Cretaceous. Paleoceanography 17, 3.
Ma, C., Meyers, S.R., Sageman, B.B., Singer, B.S., Jicha, B.R., 2014. Testing the astronomical time scale for Oceanic Anoxic Event 2, and its extension into Cenomanian strata of the Western Interior Basin. Geol. Soc. Am. Bull. 126, 974–989.
MacLeod, K.G., Marin, E.E., Blair, S.W., 2008. Nd excursions across the Cretaceous oceanic anoxia event 2 (Cenomanian–Turonian) in the tropical North Atlantic. Geology 36, 811–814.
Martin, E.E., MacLeod, K.G., Jimenez Berrocso, A., Bourbon, E., 2012. Water mass circulation on Demerara Rise during the Late Cretaceous based on Nd isotopes. Earth Planet. Sci. Lett. 327–328, 111–120.
Mattinson, J.M., 2005. Zircon U–Pb chemical abrasion ("CA-TIMS") method: combined annealing and multi-step partial dissolution analysis for improved precision and accuracy of zircon ages. Chem. Geol. 220, 47–66.
McArthur, J.M., Howarth, R.J., Bailey, T., 2004. Strontium isotope stratigraphy. In: Gradstein, F., Ogg, J., Smith, A. (Eds.), A Geological Time Scale 2004. Cambridge University Press, Cambridge, U.K., pp. 96–105.
McLean, N., Bowring, J., Bowring, S., 2011. An algorithm for U–Pb isotope dilution data reduction and uncertainty propagation. Geochem. Geophys. Geosyst. 12. QOAA18.
McLean, N., Condon, D.J., Schoene, B., Bowring, S.A., 2015. Evaluating uncertainties in the calibration of isotopic reference materials and multi-element isotopic tracers (EARTHTIME Tracer Calibration Part II). Geochim. Cosmochim. Acta. http://dx.doi.org/10.1016/j.gca.2015.02.040.
Meyers, S.R., Siewert, S.E., Singer, B.S., Sageman, B.B., Condon, D.J., Obradovich, J.D., Jicha, B.R., Sawyer, D.A., 2012a. Intercalibration of radioisotopic and astrochronologic time scales for the Cenomanian–Turonian boundary interval, Western Interior Basin, USA. Geology 40, 7–10.
Meyers, S.R., Sageman, B.B., Arthur, M.A., 2012b. Obliquity forcing and the amplification of high-latitude climate processes during Oceanic Anoxic Event 2. Paleoceanography 27, PA3212. http://dx.doi.org/10.1029/2012PA002286.
Montoya-Pino, C., Weyer, S., Anbar, A.D., Pross, J., Oschmann, W., van de Schootbrugge, B., Arz, H.W., 2010. Global enhancement of ocean anoxia during Oceanic Anoxic Event 2: a quantitative approach using U isotopes. Geology 38, 315–318.
Mort, H.P., Adatte, T., Follmi, K.B., Keller, G., Steinmann, P., Matera, V., Berner, Z., Stüben, D., 2011. Phosphorus and the roles of productivity and nutrient recycling during Ocenic Anoxic Event 2. Geology 35 (6), 483–486.
Murphy, M.A., Rodda, P.U., Morton, D.M., 1969. Geology of the Ono Quadrangle, Shasta and Tehama Counties, California. California Division of Mines and Geology, San Francisco, CA. Bulletin 192.
Owens, J.D., Gill, B.C., Jenkyns, H.C., Bates, S.M., Severmann, S., Kuypers, M.M.M., Woodfine, R.G., Lyons, T.W., 2013. Sulfur isotopes track the global extent and dynamics of euxinia during Cretaceous Oceanic Anoxic Event. Proc. Natl. Acad. Sci. USA 110, 18407–18412. http://dx.doi.org/10.1073/pnas.1305304110.
Oxburgh, R., 2001. Residence time of osmium in the oceans. Geochem. Geophys. Geosyst. 2, 2000GC000104.
Paquay, F.S., Ravizza, G., 2012. Heterogeneous seawater $^{187}Os/^{188}Os$ during the Late Pleistocene glaciations. Earth Planet. Sci. Lett. 349–350, 126–138.
Peucker-Ehrenbrink, B., Jahn, B., 2001. Rhenium–osmium isotope systematics and platinum group element concentrations: loess and the upper continental crust. Geochem. Geophys. Geosyst. (ISSN 1525-2027) 2.
Peucker-Ehrenbrink, B., Ravizza, G., 2000. The marine osmium isotope record. Terra Nova 12, 205–219.
Pogge von Strandmann, P.A.P., Jenkyns, H.C., Woodfine, R.G., 2013. Lithium isotope evidence for enhanced weathering during Oceanic Anoxic Event 2. Nat. Geosci. 6, 668–672.
Pratt, L.M., Kauffman, E.G., Zelt, F.B., 1985. Fine-grained deposits and biofacies of the Cretaceous Western Interior Seaway: evidence for cyclic sedimentary processes. In: Midyear Meeting. In: Soc. Econ. Paleont. Miner. Field Trip Guidebook, vol. 4. Golden, Colorado.
Quidelleur, X., Paquette, J.L., Fiet, N., Takashima, R., Tiepolo, M., Desmares, D., Nishi, H., Grosheny, D., 2011. New U–Pb (ID-TIMS and LA-ICPMS) and $^{40}Ar/^{39}Ar$ geochronological constraints of the Cretaceous geologic time scale calibration from Hokkaido (Japan). Chem. Geol. 286, 72–83.
Rooney, A.D., Chew, D., Selby, D., 2011. Re–Os geochronology of the Neoproterozoic – Cambrian Dalradian Supergroup of Scotland and Ireland: implications for Neoproterozoic stratigraphy, glaciations and Re–Os systematics. Precambrian Res. 185, 202–214.
Sageman, B.B., Meyers, S.R., Arthur, M.A., 2006. Orbital time scale and new C-isotope record for Cenomanian–Turonian boundary stratotype. Geology 34, 125–128.
Sageman, B.B., Singer, B.S., Meyers, S.R., Siewart, S.E., Walaszczyk, I., Condon, D.J., Jicha, B.R., Obradovich, J.D., Sawyer, D.A., 2014. Integrating $^{40}Ar/^{39}Ar$, U–Pb, and astronomical clocks in the Cretaceous Niobrara Formation, Western Interior Basin, USA. Geol. Soc. Amer. Bull. http://dx.doi.org/10.1130/B30929.1.

Schlanger, S.O., Arthur, M.A., Jenkyns, H.C., Scholle, P.A., 1987. The Cenomanian/Turonian Oceanic Anoxic Event, I. Stratigraphy and distribution of organic carbon-rich beds and the marine $\delta^{13}C$ excursion. In: Brooks, J., Fleet, A.J. (Eds.), Marine Petroleum Source Rocks. In: Spec. Publ., vol. 26. Geological Society, London, pp. 371–399.

Selby, D., Creaser, R.A., 2003. Re–Os geochronology of organic rich sediments: an evaluation of organic matter analysis methods. Chem. Geol. 200, 225–240.

Snow, L.J., Duncan, R.A., Bralower, T.J., 2005. Trace element abundances in the Rock Canyon Anticline, Pueblo, Colorado, marine sedimentary section and their relationship to Caribbean plateau construction and oxygen anoxic event 2. Paleoceanography 20. http://dx.doi.org/10.1029/2004PA001093.

Takashima, R., Kawabe, F., Nishi, H., Moriya, K., Wani, R., Ando, H., 2004. Geology and stratigraphy of forearc basin sediments in Hokkaido, Japan: cretaceous environmental events on the northwest Pacific margin. Cretac. Res. 25, 365–390.

Takashima, R., Nishi, H., Yamanaka, T., Hayashi, K., Waseda, A., Obuse, A., Tomosugi, T., Deguchi, N., Mochizuki, S., 2010. High-resolution terrestrial carbon isotope and planktic foraminiferal records of the Upper Cenomanian to the Lower Campanian in the Northwest Pacific. Earth Planet. Sci. Lett. 289, 570–582.

Takashima, R., Nishi, H., Yamanaka, T., Tomosugi, T., Fernando, A.G., Tanabe, K., Moriya, K., Kawabe, F., Hayashi, K., 2011. Prevailing oxic environments in the Pacific Ocean during the mid-Cretaceous Oceanic Anoxic Event 2. Nat. Commun. 2, 234. http://dx.doi.org/10.1038/ncomms1233.

Tamaki, M., Itoh, Y., 2008. Tectonic implications of paleomagnetic data from upper Cretaceous sediments in the Oyubari area, central Hokkaido, Japan. Isl. Arc 17, 270–284.

Tegner, C., Storey, M., Holm, P.M., Thorarinsson, S.B., Zhao, X., Lo, C.-H., Knudsen, M.F., 2011. Magmatism and Eurekan deformation in the High Arctic Large Igneous Province: $^{40}Ar$–$^{39}Ar$ age of Kap Washington Group volcanics, North Greenland. Earth Planet. Sci. Lett. 303, 203–214.

Trabucho-Alexandre, J., Tuenter, E., Henstra, G.A., van der Zwan, K.J., van de Wal, R.S.W., Dijkstra, H.A., de Boer, P.L., 2010. The mid-Cretaceous North Atlantic nutrient trap: black shales and OAEs. Paleoceanography 25. http://dx.doi.org/10.1029/2010PA001925.

Tsikos, H., Jenkyns, H.C., Walsworth-Bell, B., Petrizzo, M.R., Forster, A., Kolonic, S., Erba, E., Premoli-Silva, I.P., Baas, M., Wagner, T., Sinninghe Damsté, J.S., 2004. Carbon-isotope stratigraphy recorded by the Cenomanian–Turonian Oceanic Anoxic Event: correlation and implications based on three key localities. J. Geol. Soc. (Lond.) 161, 711–719.

Turgeon, S.C., Creaser, R.A., 2008. Cretaceous Anoxic Event 2 triggered by a massive magmatic episode. Nature 454, 323–326.

Voigt, S., Erbacher, J., Mutterlose, J., Weiss, W., Westerhold, T., Wiese, F., Wilmsen, M., Wonik, T., 2008. The Cenomanian–Turonian of the Wunstorf section (North Germany): global stratigraphic reference section and new orbital time scale for Oceanic Anoxic Event 2. Newsl. Stratigr. 43, 65–89.

Wendt, I., Carl, C., 1991. The statistical distribution of the mean squared weighted deviation. Chem. Geol., Isot. Geosci. Sect. 86, 275–285.

Zheng, X.-Y., Jenkyns, H.C., Gale, A.S., Ward, D.J., Henderson, G.M., 2013. Changing ocean circulation and hydrothermal inputs during Ocean Anoxic Event 2 (Cenomanian–Turonian): evidence from Nd-isotopes in the European shelf sea. Earth Planet. Sci. Lett. 375, 338–348. http://dx.doi.org/10.1016/j.epsl.2013.05.053.